

Article

# Antisolvent Sonocrystallisation of Sodium Chloride and the Evaluation of the Ultrasound Energy Using Modified Classical Nucleation Theory

Judy Lee <sup>1,2,\*</sup>  and Shanshan Yang <sup>2</sup><sup>1</sup> Department of Chemical and Process Engineering, University of Surrey, Surrey GU27XH, UK<sup>2</sup> Department of Chemical and Biomolecular Engineering, University of Melbourne, Melbourne 3010, Australia; youngbby@hotmail.com

\* Correspondence: j.y.lee@surrey.ac.uk

Received: 30 July 2018; Accepted: 8 August 2018; Published: 10 August 2018



**Abstract:** The crystal nucleation rate of sodium chloride in ethanol was investigated by measuring the induction time at various supersaturation ratios under silent and ultrasound irradiation at frequencies between 22 and 500 kHz. Under silent conditions, the data follows the classical nucleation theory showing both the homogeneous and heterogeneous regions and giving an interfacial surface tension of 31.0 mN m<sup>-2</sup>. Sonication led to a non-linearity in the data and was fitted by a modified classical nucleation theory to account for the additional free energy being supplemented by sonication. For 98 kHz, this free energy increased from 1.33 × 10<sup>8</sup> to 1.90 × 10<sup>8</sup> J m<sup>-3</sup> for sonication powers of 2 to 15 W, respectively. It is speculated that the energy was supplemented by the localised bubble collapses and collisions. Increasing the frequency from 22 to 500 kHz revealed that a minimum induction time was obtained at frequencies between 44 and 98 kHz, which has been attributed to the overall collapse intensity being the strongest at these frequencies.

**Keywords:** sonocrystallisation; antisolvent; ultrasound; acoustic cavitation; induction time; classical nucleation theory; free energy

## 1. Introduction

Crystallisation is an operation commonly adopted by the chemical and pharmaceutical industries for separation and purification processes [1]. For solutes that are heat sensitive, antisolvent crystallisation is preferred as it allows processes to be conducted at a constant temperature, and is both convenient and economical. However, this approach sometimes suffers from long induction times, broad particle size distributions, asymmetrical crystal morphology and product purity [2]. Ultrasound has been shown to facilitate the nucleation of crystals, reduce the induction time ( $t_{ind}$ ) in a controlled and reproducible way to generate narrower size distribution products, and selectively crystallise a specific polymorph [3–11]. However, the mechanism behind ultrasound-induced nucleation is still contentious [12–14] as studies have shown that ultrasound increases induction time [15] and promotes crystal growth [16].

It is well accepted that cavitation bubbles generated by the ultrasound influence the crystallisation process [4,17–22]. However, the complexity of both the cavitation and crystallisation processes, which occur in extremely short time and length scales, makes it difficult to determine the precise mechanism behind sonocrystallisation. The application of the classical nucleation theory (CNT) of crystallisation to examine the effects of ultrasound are limited [3,23–27]. In CNT, the change in the free energy,  $\Delta G(r)$  [J], for the formation of a spherical cluster of radius  $r$  [m] is described by Equation (1a).  $\Delta G(r)$  is the

sum of the interfacial free energy to create a surface and the bulk free energy,  $\Delta G_v$  [ $\text{J m}^{-3}$ ], associated with phase change:

$$\Delta G(r) = 4\pi r^2 \gamma + \frac{4\pi r^3}{3} (\Delta G_v) \quad (1a)$$

$$\Delta G_v = - \left( \frac{vRT \ln(S)}{V_m} \right) \quad (1b)$$

In Equation (1a),  $r$  is assumed to be spherical and  $\gamma$  [ $\text{J m}^{-2}$ ] is the solution crystal interfacial tension. In Equation (1b),  $S$  is the supersaturation ratio,  $v$  is the number of mols of ions formed from one mole of electrolyte (which is two for NaCl),  $R$  is the ideal gas constant [ $8.314 \text{ J K}^{-1} \text{ mol}^{-1}$ ],  $T$  is the temperature [293 K], and  $V_m$  is the molar volume [ $2.7 \times 10^{-5} \text{ m}^3 \text{ mol}^{-1}$ ]. Equation (1a) is then used to determine the critical free energy barrier ( $\Delta G_{crit}$ ) and critical cluster radius ( $r_c$ ) necessary for stable crystal nuclei to occur, which is known as nucleation. The nucleation rate ( $J$ ) of this process can be described by an Arrhenius-type expression [28]:

$$J = A \exp\left(\frac{-\Delta G_{crit}}{k_B T}\right) \quad (2)$$

where  $A$  is the pre-exponential factor that is related to the solute diffusivity in solution and  $k_B$  is the Boltzmann constant [ $1.38 \times 10^{-23} \text{ m}^2 \text{ kg s}^{-2} \text{ K}^{-1}$ ]. The  $t_{ind}$  [s], which is the time between the establishment of supersaturation and when the crystals are first detected, can be taken as inversely proportional to the nucleation rate [29] to give:

$$\ln(t_{ind}) = \ln\left(\frac{1}{A}\right) + \frac{16\pi\gamma^3}{3k_B T \left(\frac{-vRT \ln(S)}{V_m}\right)^2} \quad (3)$$

Equation (3) has been used to investigate the effect of ultrasound on the linear relationship between  $\ln(t_{ind})$  and  $1/\ln^2(S)$ . Lyczko et al. [3] reported a decrease in the slope of this linear relationship with sonication, indicating a lowering of the solution-crystal surface tension suggesting that ultrasound increases the heterogeneity of the system. The intercept of the linear slope showed no trend with increasing sonication. In contrast to this, others have found no change in the slope [24,25] but observed a decrease in the intercept,  $\ln(1/A)$ , or an increase in  $A$  with increasing sonication intensity, implying that ultrasound accelerates the diffusion of solutes from the bulk of the fluid through the stagnant film to the solid surface [25].

According to the CNT, the system needs to overcome the critical energy barrier for crystal nucleation to occur. It has been reported that there exists a certain threshold of ultrasound energy for the activation of primary nucleation, and below which nucleation is hindered [15,30]. The ultrasound energy is often quantified via calorimetric measurements, which measure the dissipated heat and do not always correlate directly to the cavitation activity. Furthermore, most of the sonocrystallisation studies, including those mentioned above, have used 20 kHz power ultrasonic horns that generate intense bulk fluid shear and heating in addition to cavitation, which are usually localised near the horn tip [31]. This would make it even more difficult to directly link calorimetric power to cavitation activity and cavitation activity to crystallisation. The intense local shear created by the horn can also significantly affect crystallisation, especially in antisolvent crystallisation processes, making it challenging to determine the role that cavitation bubbles play. Plate transducers, similar to ultrasonic horns, generate cavitation bubbles and have been shown to induce crystallisation effects similar to those produced by the ultrasonic horn [9]. Unlike the ultrasonic horn, the intensity of the ultrasound from plate transducers is not localised but distributed throughout the liquid with cavitation activity located at pressure antinodes (Figure 1). Furthermore, plate transducers do not generate the intense heating, shearing, and bulk fluid mixing that are observed with ultrasonic horns.

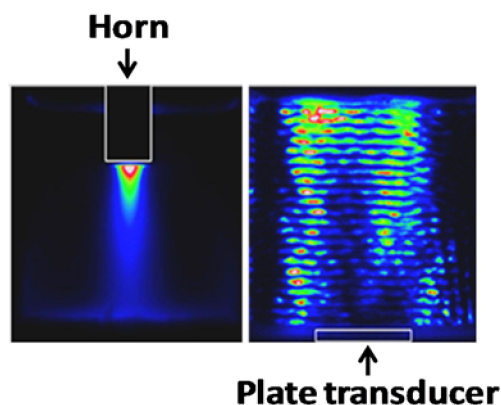


**Figure 1.** Spatial distribution of cavitation bubbles generated by an ultrasonic horn (**left**) and 168 kHz frequency plate transducer (**right**). Image adapted from [32] with permission from © Springer Science + Business Media Singapore 2018 and the colours were arbitrarily added to indicate the sonoluminescence emission captured.

The focus of this study is to use plate transducers of various frequencies to investigate the induction time of sodium chloride in ethanol and report, for the first time, the application of a modified CNT to better quantify ultrasound energy.

## 2. Experimental Details

### 2.1. Materials

Sodium chloride (NaCl, 99.5%) was purchased from Merck (Darmstadt, Germany) and 100% absolute ethanol was purchased from Chem-Supply (Adelaide, Australia). They were used as received without further purification. All solutions were made using purified water with a resistivity greater than 18.2 M $\Omega$  cm.

### 2.2. Supersaturation Ratio

The antisolvent crystallisation of NaCl from a water-ethanol-NaCl ternary system was carried out by the addition of aqueous NaCl-water solution to 300 g of ethanol to give a specific supersaturation ratio. The mass of the aqueous NaCl-water added was fixed at 15 g to keep the mass ratio of ethanol to aqueous solution constant. For consistency, the concentration of NaCl was varied by diluting various aliquots of 200 g L<sup>-1</sup> NaCl stock solution to make up a final mass of NaCl-water solution of 15 g. To determine the solubility of NaCl in 95.2 wt % of ethanol, 15 g of 200 g L<sup>-1</sup> NaCl was added to 300 g of ethanol. When all the NaCl had precipitated, the solution was filtered (0.45  $\mu$ m) and a known amount of the saturated solution was evaporated to determine the amount of NaCl dissolved. The solubility of NaCl in 95.2 wt % of ethanol was found to be 1.63  $\pm$  0.24 g kg<sup>-1</sup> solution.

### 2.3. Sonocrystallisation Process

All antisolvent crystallisation experiments were performed in a cylindrical Pyrex cell with an internal diameter of 6.2 cm and height of 11.2 cm and with the ultrasound transducer located at the bottom (Figure 2). A Langevin-type multi-frequency transducer with a diameter of 4.5 cm (resonance frequencies: 22, 44, 98 and 139 kHz, Honda Electric, Tokyo, Japan) and a 500 kHz piezo-electric ceramic plate transducer were powered by an amplifier (AG 1006, T&C Power Conversion, New York, NY, USA). The power quoted in this work will be the unit electrical power output unless stated otherwise.

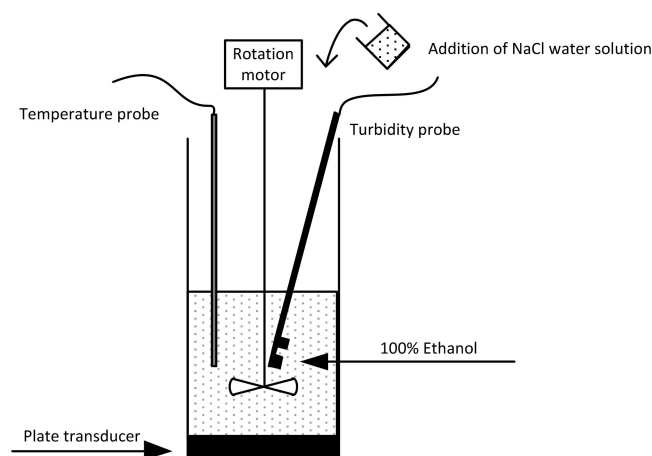


**Figure 2.** A schematic diagram of the setup used in this study.

An overhead stirrer operating at 100 rpm was used for all sonication experiments to ensure the solution was well mixed and NaCl crystals were in suspension. The addition of NaCl was performed by simply pouring the solution into the cell containing the antisolvent (addition time was less than 2 s). All experiments were performed at a temperature of  $20 \pm 0.5$  °C and with at least three independent repeats to ensure reproducibility.

#### 2.4. Induction Time Measurements

The turbidity of the solution was measured as a function of time (data collected at 1 s intervals) using a fibre-optic turbidity probe (Crystal Eyes, H.E.L. Limited, Hertfordshire, UK) and the induction time determined by the time lapse between the addition of the NaCl-water solution and the onset of turbidity. The turbidity can be affected by the initial degassing of the ethanol with the addition of concentrated salt solution and the cavitation bubbles from the ultrasound. Therefore, the onset of turbidity was determined by taking the intercept of the slope of the initial linear rise in the turbidity and the initial blank turbidity reading of ethanol solution before the addition of the salt solution (see Figure S1 in Supplementary Information). A data table for all the induction times measured at different supersaturation ratios and experimental conditions can be found in Tables S1–S9 in the Supplementary Information.

#### 2.5. Modification of the Classical Nucleation Theory (CNT)

Following the method outlined by Alexander et al. [33] for the determination of the reduction in the free energy brought about by the isotropic electronic polarisation of subcritical crystal nuclei by laser radiation, Equation (1a) is modified to include the additional energy for nucleation supplemented by ultrasound ( $\Delta W_U$ ):

$$\Delta G = 4\pi r^2 \gamma + \frac{4\pi r^3}{3} (\Delta G_v + \Delta W_U) \quad (4)$$

The  $\Delta G_{crit}$  is determined by minimising the free energy function in Equation (4) to give:

$$\Delta G_{crit} = \frac{16\pi\gamma^3}{3(\Delta G_v + \Delta W_U)^2} \quad (5)$$

Using Equation (2), the relationship between the induction time in the presence of ultrasound  $\ln(t_{ind})$  and  $1/\ln^2(S)$  is:

$$\ln(t_{ind}) = \ln\left(\frac{1}{A}\right) + \frac{16\pi\gamma^3}{3k_B T \left(\frac{-vRT \ln(s)}{V_m} + \Delta W_U\right)^2} \quad (6)$$

In the absence of ultrasound ( $\Delta W_U = 0$ ), Equation (6) reduces to Equation (3). Using the Matlab nonlinear least-squares solver, Equation (6) was fitted to the data to determine the best-fit parameters  $A$  and  $\Delta W_U$ .

### 3. Results and Discussion

#### 3.1. Absence of Ultrasound

In the absence of ultrasound, the measured induction time increased with decreasing supersaturation ratio, as expected. When plotted in terms of  $\ln(t_{ind})$  as a function of  $1/\ln^2(S)$  (Figure 3), two distinct linear slopes are observed. At high supersaturation ratios, or low  $1/\ln^2(S)$ , homogeneous nucleation occurs and according to CNT the linear slope can be fitted with Equation (3) to yield  $A$  and  $\gamma$  to 1.22 and  $31.0 \text{ mN m}^{-2}$ , respectively. This surface tension value is comparable with those reported in the literature for NaCl:  $25.6 \text{ mN m}^{-2}$  [34] and  $38 \text{ mN m}^{-2}$  [35]. At low supersaturation ratios, or high  $1/\ln^2(S)$ , a lower gradient slope is observed. This is indicative of heterogeneous nucleation occurring because at a given supersaturation, any impurities or surfaces in the system can initiate crystal nucleation by decreasing  $\gamma$  and result in a shorter induction time compared to a pure homogeneous system [28].

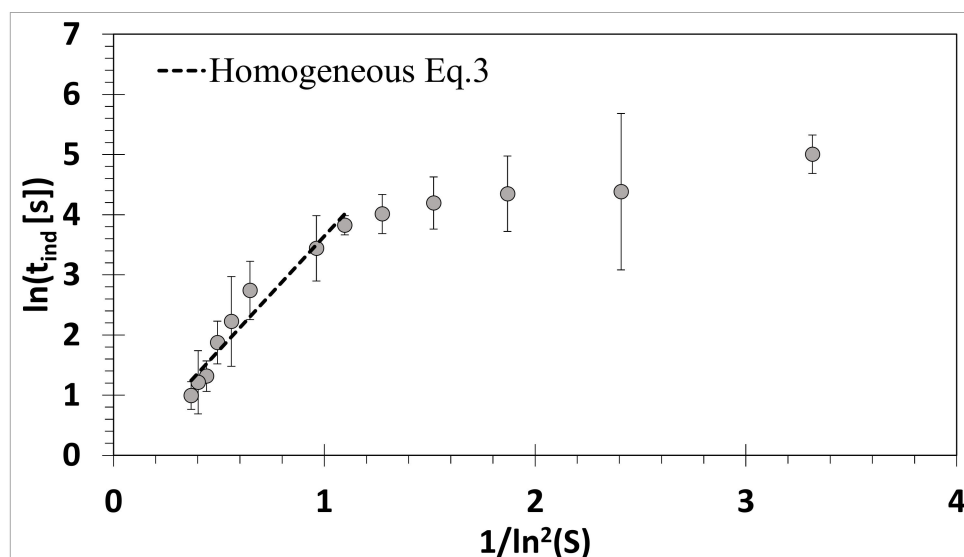


**Figure 3.**  $\ln(t_{ind})$  in the absence of ultrasound plotted as a function of  $1/\ln^2(S)$  showing two linear regions denoting the homogeneous and heterogeneous nucleation. Equation (3), which is only valid for homogeneous nucleation, is fitted to the data. A stirring speed of 100 rpm was used.

Crystallisation, especially antisolvent crystallisation, is sensitive to stirring and stirring speed [9,36,37]. The acoustic pressure gradient, as well as cavitation bubbles, can induce both bulk and localised fluid movements [38–40]. Different stirring speeds were applied to eliminate the additional bulk stirring effect brought about by ultrasound. As can be seen in Figure 4, a stirring speed of 100 rpm was adequate, and any stirring speed above 100 rpm had a negligible effect on the induction time, except at very low supersaturation ratios.

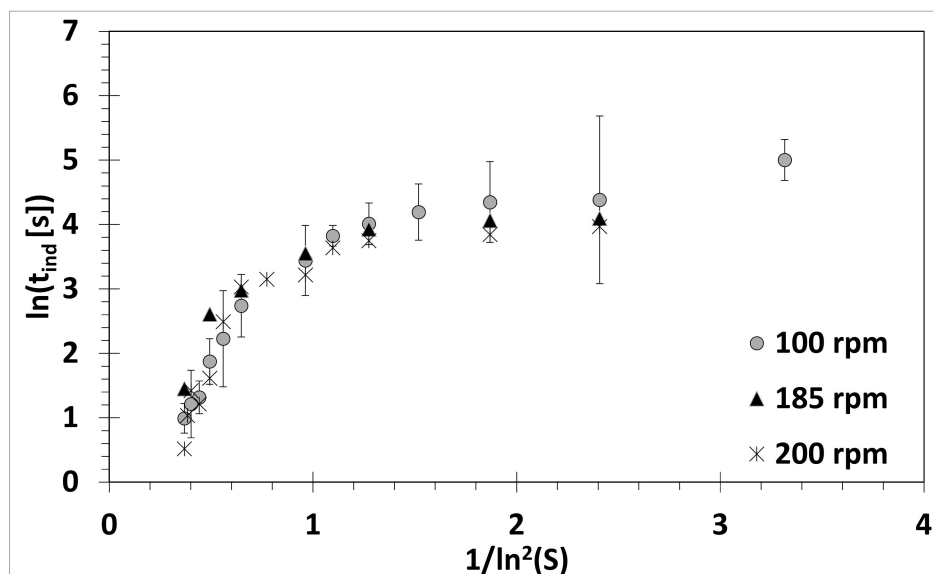


**Figure 4.**  $\ln(t_{ind})$  in the absence of ultrasound plotted as a function of  $1/\ln^2(S)$  for different stirring speeds.

### 3.2. Influence of Ultrasound

The influence of sonication on the induction time is shown in Figure 5, which agrees with what has been reported in the literature [3,6,24,25]: Sonication can significantly reduce the induction time and this reduction increases with decreasing supersaturation ratio. The effect of different sonication powers is more pronounced when the data is plotted in terms of  $\ln(t_{ind})$  as a function of  $1/\ln^2(S)$  (Figure 6). A decrease in the induction time is seen with increasing sonication power. With sonication, the two homogeneous and heterogeneous regions are less obvious, with the induction times at low supersaturation being reduced to that comparable to the induction times observed during homogeneous nucleation. If ultrasound was affecting parameters such as  $T$  and  $S$ , then one would expect the data obtained under sonication to shift from the silent condition but still exhibit the two linear regions. Non-linearity has been observed for agitated systems and attributed to heterogeneous or a secondary mode of nucleation [36]. However, it was demonstrated (Figure 4) that a stirring speed of 100 rpm was above the critical speed at which the induction time was no longer affected by bulk stirring at a macroscopic level. Therefore, it was assumed that the influence of ultrasound was at a microscopic level, relating to either primary or secondary nucleation rather than heterogeneous nucleation. This is consistent with the findings reported by Guo et al. [23,24] and Miyasaka et al. [30]. This assumption was further confirmed by setting  $\gamma$  in Equation (6) as a variable along with  $A$  and  $\Delta W_U$ , where the numerical results obtained were inconsistent with experimental data (see Supplementary Information). For these reasons,  $\gamma$  was assumed to be the same as in the silent condition.

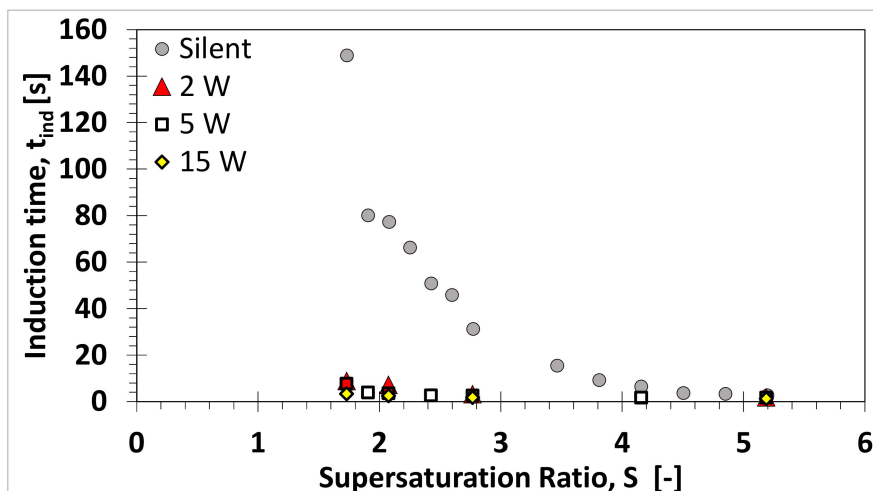


**Figure 5.** Induction time  $t_{ind}$  as a function of supersaturation ratio for silent and presence of ultrasound (98 kHz) at three different power levels.

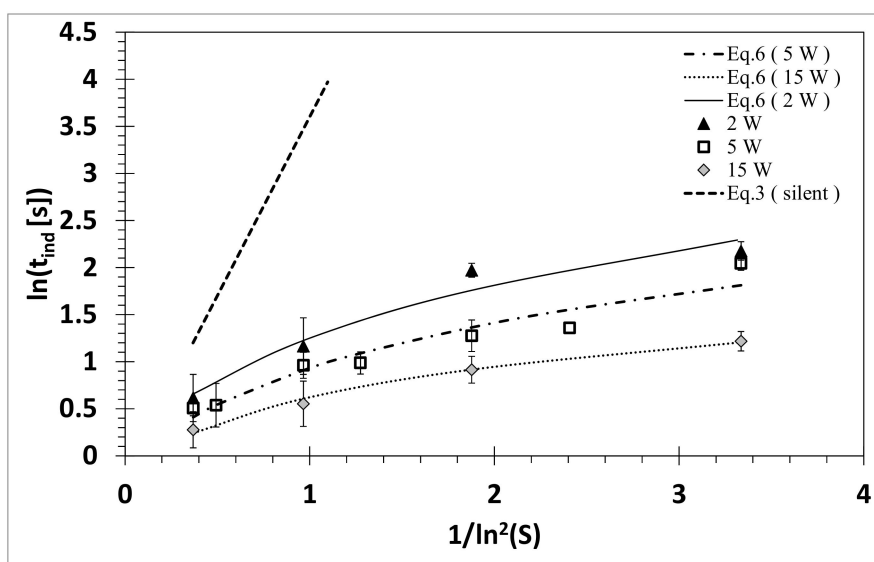


**Figure 6.**  $\ln(t_{ind})$  plotted as a function of  $1/\ln^2(S)$  for 98 kHz at different ultrasound powers and the data were fitted with Equation (6). Equation (3) in Figure 2 for no ultrasound is inserted for comparison.

Separating secondary from primary nucleation is difficult. Therefore, it was assumed that homogeneous nucleation is the dominating mechanism during sonication and the deviation from linearity was due to the additional  $\Delta W_U$  in Equation (6). Assuming  $\gamma$  and  $S$  to be unaffected by ultrasound, the data was then fitted with Equation (6) to obtain  $A$  and  $\Delta W_U$  numerically (Table 1). The values show that the application of only 2 W of ultrasound was able to decrease the free energy for nucleation by  $1.33 \times 10^8 \text{ J m}^{-3}$ . This is in the same order of magnitude as the free energy for phase transformation ( $\Delta G_v$ ), which varies from  $-9.91 \times 10^7 \text{ J m}^{-3}$  to  $-2.97 \times 10^8 \text{ J m}^{-3}$  for supersaturation ratios of 1.73 to 5.20, respectively. Increasing the sonication power further decreased the free energy but at a smaller extent compared to 2 W. The pre-exponent value is similar to that obtained in the absence of ultrasound, suggesting that ultrasound was not affecting the diffusion of solutes from the bulk of the fluid through the stagnant film to the solid surface. This differs from the study by Guo et al. where they fitted Equation (3) and observed a decrease in the pre-exponent with increasing power for barium sulphate [25] and roxithromycin [24] while the other parameters remained constant or had an insignificant change in the presence of ultrasound. The different observations could be

attributed to the reactive crystallisation of barium sulphate and roxithromycin being an organic material. An inorganic salt, potassium sulphate, was investigated by Lyczko et al. [3] and their data fitted with Equation (3). They found that both the pre-exponent and surface tension term changed with sonication, leading to the conclusion that ultrasound induces heterogeneous nucleation. In that study, a cooling crystallisation system was investigated at a fixed stirring speed and it is uncertain whether sonication could have contributed to the mixing effect. In addition, it was reported later that the solubility of potassium sulphate is sensitive to pressure [6] with an increase of 3 kBar decreasing the solubility by 30%; for the sodium chloride used in this study, the solubility would only decrease by 0.02% [41]. Further support that the effect of ultrasound on cooling crystallisation of an organic material may occur via a different mechanism compared to antisolvent crystallisation of an inorganic salt is given by Kordylla [26]. In that report, they demonstrated, using a simulation model of cooling crystallisation of dodecanedioic acid, an organic material, that the influence of ultrasound is via a heterogeneous nucleation mechanism.

**Table 1.**  $\Delta W_U$  and the pre-exponent A, determined by fitting Equation (6) to the experimental data shown in Figure 6 for different ultrasound powers. It was assumed  $\gamma = 31.0 \text{ mNm}^{-2}$  and that the supersaturation ratio is unaffected by ultrasound. The pre-exponent A, obtained using Equation (3) for the absence of ultrasound, is also shown for comparison.

Amplifier Power [W]	Calorimetric Power [W]	$\Delta W_U [\text{J m}^{-3}]$	A
0	0	0	1.22
2	0.73	$-1.33 \times 10^8$	1.01
5	1.8	$-1.48 \times 10^8$	1.24
15	5.5	$-1.90 \times 10^8$	1.32

To illustrate the effect of ultrasound on the free energy of nucleation and critical cluster radius, the theoretical plot of Equation (4) as a function of the cluster radius is shown in Figure 7. Figure 7a shows that under silent conditions, increasing the supersaturation ratio decreases the  $\Delta G_{crit}$  as well as the  $r_c$ , allowing much smaller clusters to continue to grow rather than dissolve away. A similar decrease in  $\Delta G_{crit}$  and  $r_c$  with an increasing supersaturation ratio is observed at a fixed acoustic power of 2 W, but at a much lower  $\Delta G_{crit}$  and smaller  $r_c$ . At a given supersaturation ratio, increasing the applied acoustic power has a similar effect on the  $\Delta G_{crit}$  and  $r_c$  as increasing the supersaturation ratio (Figure 7b).

Although the theoretical fit of Equation (6) allows one to quantify the effect of ultrasound on the crystallisation process, the direct mechanism is more difficult to determine. Equation (6) was used by Alexander et al. [33] to account for the additional energy supplied by a laser to nucleate an aqueous supersaturated solution of potassium chloride. In that study, the additional energy was linked to the isotropic electronic polarisation of the subcritical crystal nuclei by the electric field of the light. The supplementary energy supplied by ultrasound could come from the localised intense asymmetric collapse of bubbles, as suggested by Lee et al. [17]. The antisolvent crystallisation of sodium chloride was readily observed from a cluster of cavitation bubbles (Figure 8) and the violent collision between bubbles brought together by the Bjerknes forces [17].

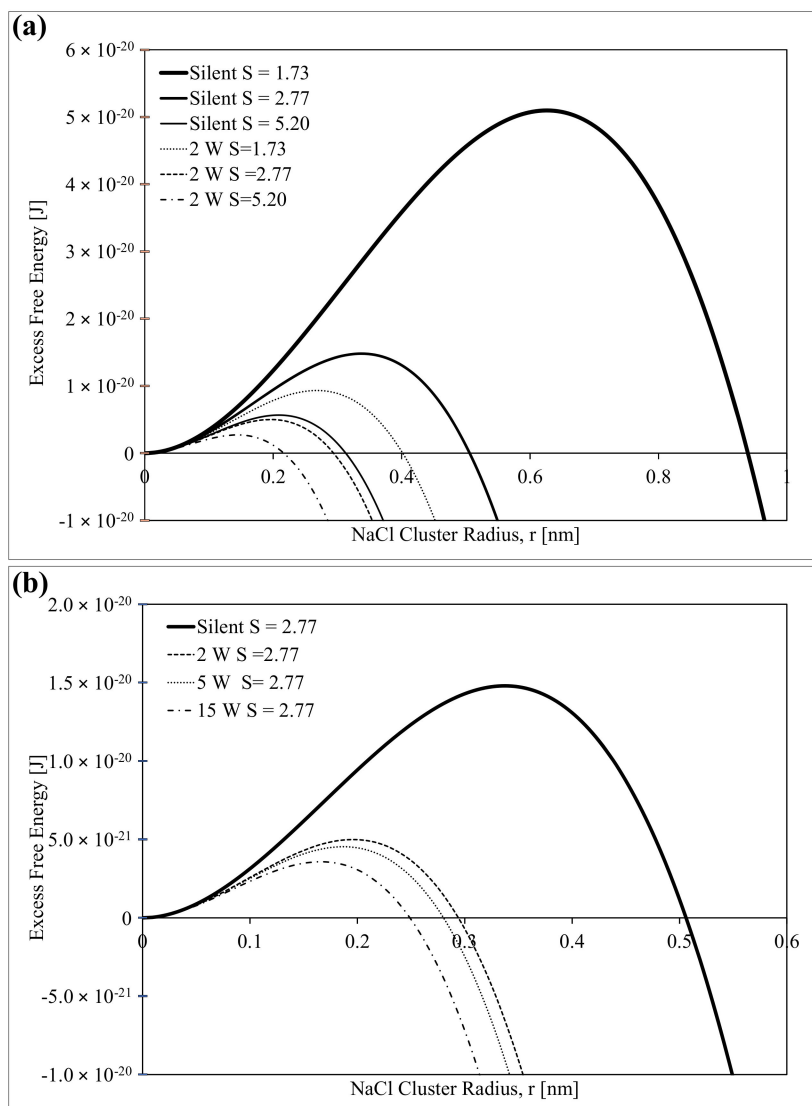


**Figure 7.** Calculated free energy as a function of nucleus radius for (a) various supersaturation ratios under silent and 2 W sonication, and (b) various sonication powers at a fixed supersaturation ratio.

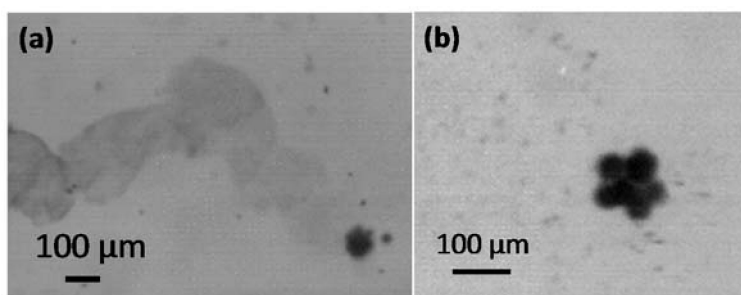


**Figure 8.** (a) Images of a trail of sodium chloride crystals being left behind in the wake of a moving cluster of cavitating bubbles; (b) Enlarged image showing sodium chloride crystals being emitted from the cavitation bubble cluster during sonocrystallisation. Cavitation was generated by a 33.1 kHz plate transducer. Adapted with permission from [17]. Copyright (2018) American Chemical Society.

The overall energy supplemented by the collapsing cavitation bubbles would depend on the collapse intensity of an individual bubble and the cavitation bubble population, which can be tuned

by varying the frequency. The induction times as a function of ultrasound frequency at different supersaturation ratios are plotted in Figure 9. It can be observed for all supersaturation ratios that as the frequency increases the induction time decreases to a minimum frequency around 44–98 kHz. As the frequency increases further to 500 kHz, sonication is less effective and the induction time approaches that of the silent condition. This optimum frequency around 44–98 kHz agrees with previously reported frequency studies [17,21]. As the frequency increases, the wavelength of the acoustic waves becomes shorter and this can increase the number of antinodes resulting in an increase in the population of sonoluminescing bubbles [42]. However, at the same time, studies have shown that increasing the frequency reduces the strength of the pressure standing wave [38,40], resulting in lower cavitation activity in the system. Increasing the frequency will also decrease the size of the cavitation bubbles [43], leading to a weaker collapse intensity [44]. It is this balance between the increase in the number of cavitation bubbles and the decrease in the bubble collapse intensity as the frequency increases that gives rise to the observed optimum sonocrystallisation effect between 44 and 98 kHz.

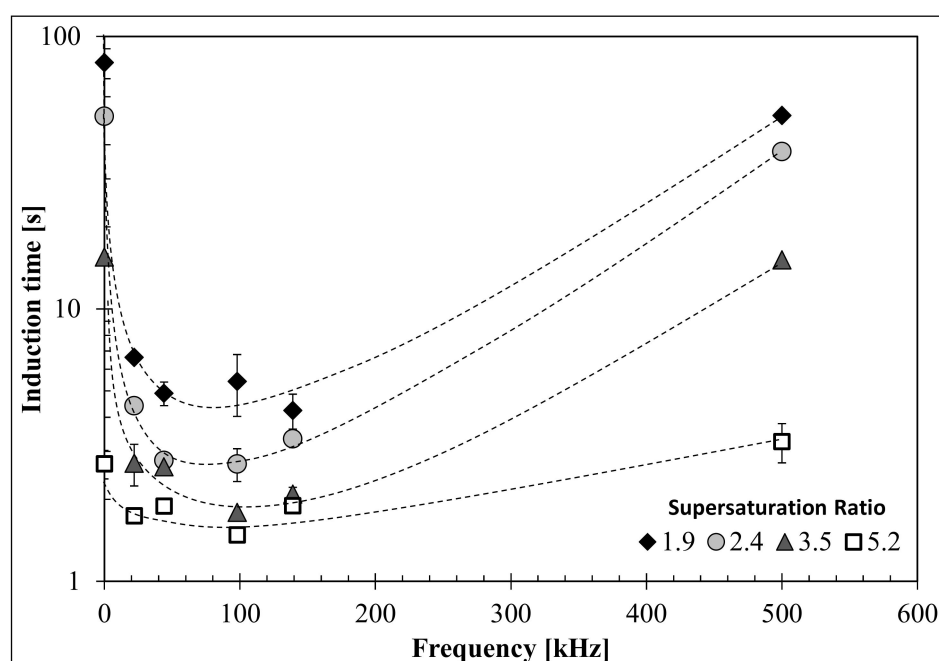


**Figure 9.** Induction time as a function of sonication frequency for different supersaturation ratios. For all the frequencies the calorimetric power and stirring speed were fixed at a calorimetric power of 1.87 W and 100 rpm, respectively. The dotted lines have been drawn to guide the eye.

#### 4. Conclusions

In this study, the induction times of sodium chloride in ethanol under different supersaturation ratios were measured under silent and sonication conditions. Sonication between 2 and 15 W at 98 kHz was found to reduce the induction time significantly. The classical nucleation theory was modified and numerically fitted to the data for the first time to determine the phenomenological value of the pre-exponent  $A$  and the additional free energy from the ultrasound. The results show that the pre-exponent  $A$  was not substantially affected by sonication. However, a notable increase in supplementary free energy was observed with increasing sonication power, which would lower both the activation barrier and the critical cluster radius to result in a faster nucleation rate. The measure of induction time as a function of frequency revealed an optimum frequency between 44 and 98 kHz. A further increase to 500 kHz had very little effect on the induction time.

**Supplementary Materials:** The following are available online at <http://www.mdpi.com/2073-4352/8/8/320/s1>, Figure S1: An example of turbidity as a function of time data obtained and how induction time was determined. (a) a typical data and (b) interference from degassed bubbles when supersaturation is first established, Table S1: Induction time for different supersaturation ratios in the absence of ultrasound. A stirring speed of 100 rpm was applied, Table S2: Induction time for different supersaturation ratios in the presence of 98 kHz and 2 W sonication. A stirring speed of 100 rpm was applied, Table S3: Induction time for different supersaturation ratios in the presence of 98 kHz and 5 W sonication. A stirring speed of 100 rpm was applied, Table S4: Induction time for different supersaturation ratios in the presence of 98 kHz and 15 W sonication. A stirring speed of 100 rpm was applied, Table S5: Induction time for different supersaturation ratios in the presence of 22 kHz and 2 W sonication. A stirring speed of 100 rpm was applied, Table S6: Induction time for different supersaturation ratios in the presence of 44 kHz and 2 W sonication. A stirring speed of 100 rpm was applied, Table S7: Induction time for different supersaturation ratios in the presence of 139 kHz and 2 W sonication. A stirring speed of 100 rpm was applied, Table S8: Induction time for different supersaturation ratios in the presence of 500 kHz and 2 W sonication. A stirring speed of 100 rpm was applied, Table S9: Parameters  $\gamma$ ,  $\Delta WU$  and  $A$  for different ultrasound powers, determined by fitting Equation (6) to the data in Figure 6. It was assumed that the supersaturation ratio is unaffected by ultrasound. The pre-exponent  $A$  and  $\gamma$  obtained using Equation (3) for absence of ultrasound are also shown for comparison.

**Author Contributions:** J.L. conceptualised and designed the sonocrystallisation experiments; S.Y. performed the experiments and processed the data under J.L.'s supervision. J.L. applied the modified classical nucleation theory to the data, analysed the results, and wrote-reviewed & edited the paper.

**Funding:** This research was funded by the Australian Research Council's Discovery Early Career Research Award grant number [DE120101567].

**Acknowledgments:** We are grateful to Yos Morsi, Richard Manasseh and Jack Jiao for facilitating and assist with the use of the high-speed camera.

**Conflicts of Interest:** The authors declare no conflict of interest.

## References

1. Takiyama, H. Supersaturation operation for quality control of crystalline particles in solution crystallization. *Adv. Powder Technol.* **2012**, *23*, 273–278. [[CrossRef](#)]
2. Takiyama, H.; Otsuhata, T.; Matsuoka, M. Morphology of NaCl crystals in drowing-out precipitation operation. *Chem. Eng. Res. Des.* **1998**, *76*, 809–814. [[CrossRef](#)]
3. Lyczko, N.; Espitalier, F.; Louisnard, O.; Schwartzentruber, J. Effect of ultrasound on the induction time and the metastable zone widths of potassium sulphate. *Chem. Eng. J.* **2002**, *86*, 233–241. [[CrossRef](#)]
4. Bund, R.K.; Pandit, A.B. Sonocrystallization: Effect on lactose recovery and crystal habit. *Ultrason. Sonochem.* **2007**, *14*, 143–152. [[CrossRef](#)] [[PubMed](#)]
5. Luque de Castro, M.D.; Priego-Capote, F. Ultrasound-assisted crystallization (sonocrystallization). *Ultrason. Sonochem.* **2007**, *14*, 717–724. [[CrossRef](#)] [[PubMed](#)]
6. Harzali, H.; Baillon, F.; Louisnard, O.; Espitalier, F.; Mgaidi, A. Experimental study of sono-crystallisation of  $ZnSO_4 \cdot 7H_2O$ , and interpretation by the segregation theory. *Ultrason. Sonochem.* **2011**, *18*, 1097–1106. [[CrossRef](#)] [[PubMed](#)]
7. Price, G.; Mahon, M.F.; Shannon, J.; Cooper, C. Composition of calcium carbonate polymorphs precipitated using ultrasound. *Cryst. Growth Des.* **2011**, *11*, 39–44. [[CrossRef](#)]
8. Mori, Y.; Maruyama, M.; Takahashi, Y.; Ikeda, K.; Fukukita, S.; Yoshikawa, H.Y.; Okada, S.; Adachi, H.; Sugiyama, S.; Takano, K. Selective crystallization of metastable phase of acetaminophen by ultrasonic irradiation. *Appl. Phys. Express* **2015**, *8*, 065501. [[CrossRef](#)]
9. Lee, J.; Ashokkumar, M.; Kentish, S. Influence of mixing and ultrasound frequency on antisolvent crystallisation of sodium chloride. *Ultrason. Sonochem.* **2014**, *21*, 60–68. [[CrossRef](#)] [[PubMed](#)]
10. Bhangu, S.K.; Ashokkumar, M.; Lee, J. Ultrasound assisted crystallization of paracetamol: Crystal size distribution and polymorph control. *Cryst. Growth Des.* **2016**, *16*, 1934–1941. [[CrossRef](#)]
11. Price, C. Ultrasound—the key to better crystals for the pharmaceutical industry. *Pharm. Technol. Eur.* **1997**, *9*, 78–87.
12. Hem, S.L. The effect of ultrasonic vibrations on crystallization processes. *Ultrasonics* **1967**, *5*, 202–207. [[CrossRef](#)]
13. Zeiger, B.W.; Suslick, K.S. Sonofragmentation of molecular crystals. *J. Am. Chem. Soc.* **2011**, *133*, 14530–14533. [[CrossRef](#)] [[PubMed](#)]

14. Ratsimba, B.; Biscans, B.; Delmas, H.; Jenck, J. Sonocrystallization: The end of empiricism? *Kona Powder Part. J.* **1999**, *17*, 38–48. [[CrossRef](#)]
15. Kurotani, M.; Miyasaka, E.; Ebihara, S.; Hirasawa, I. Effect of ultrasonic irradiation on the behavior of primary nucleation of amino acids in supersaturated solutions. *J. Cryst. Growth* **2009**, *311*, 2714–2721. [[CrossRef](#)]
16. Nii, S.; Takayanagi, S. Growth and size control in anti-solvent crystallization of glycine with high frequency ultrasound. *Ultrason. Sonochem.* **2014**, *21*, 1182–1186. [[CrossRef](#)] [[PubMed](#)]
17. Lee, J.; Yasui, K.; Ashokkumar, M.; Kentish, S.E. Quantification of cavitation activity by sonoluminescence to study the sonocrystallization process under different ultrasound parameters. *Cryst. Growth Des.* **2018**. accepted. [[CrossRef](#)]
18. Grossier, R.; Louisnard, O.; Vargas, Y. Mixture segregation by an inertial cavitation bubble. *Ultrason. Sonochem.* **2007**, *14*, 431–437. [[CrossRef](#)] [[PubMed](#)]
19. Cogné, C.; Labouret, S.; Peczalski, R.; Louisnard, O.; Baillon, F.; Espitalier, F. Theoretical model of ice nucleation induced by inertial acoustic cavitation. Part 2: Number of ice nuclei generated by a single bubble. *Ultrason. Sonochem.* **2016**, *28*, 185–191. [[CrossRef](#)] [[PubMed](#)]
20. Chow, R.; Atkins, D.; Singleton, S.; Mettin, R.; Lindinger, B.; Kurz, T.; Lauterborn, W.; Povey, M.; Chivers, R. High-speed observations of the nucleation of ice by power ultrasound. *Water Prop. Food Pharm. Biol. Mater.* **2006**, *9*, 613–622.
21. Jordens, J.; Gielen, B.; Braeken, L.; Van Gerven, T. Determination of the effect of the ultrasonic frequency on the cooling crystallization of paracetamol. *Chem. Eng. Process. Process Intensif.* **2014**, *84*, 38–44. [[CrossRef](#)]
22. Rossi, D.; Jamshidi, R.; Saffari, N.; Kuhn, S.; Gavriilidis, A.; Mazzei, L. Continuous-flow sonocrystallization in droplet-based microfluidics. *Cryst. Growth Des.* **2015**, *15*, 5519–5529. [[CrossRef](#)]
23. Guo, Z.; Jones, A.G.; Li, N. Interpretation of the ultrasonic effect on induction time during BaSO<sub>4</sub> homogeneous nucleation by a cluster coagulation model. *J. Colloid Interface Sci.* **2006**, *297*, 190–198. [[CrossRef](#)] [[PubMed](#)]
24. Guo, Z.; Zhang, M.; Li, H.; Wang, J.; Kougoulos, E. Effect of ultrasound on anti-solvent crystallization process. *J. Cryst. Growth* **2005**, *273*, 555–563. [[CrossRef](#)]
25. Guo, Z.; Jones, A.G.; Li, N. The effect of ultrasound on the homogeneous nucleation of during reactive crystallization. *Chem. Eng. Sci.* **2006**, *61*, 1617–1626. [[CrossRef](#)]
26. Kordylla, A.; Krawczyk, T.; Tumačaka, F.; Schembecker, G. Modeling ultrasound-induced nucleation during cooling crystallization. *Chem. Eng. Sci.* **2009**, *64*, 1635–1642. [[CrossRef](#)]
27. Virone, C.; Kramer, H.J.M.; van Rosmalen, G.M.; Stoop, A.H.; Bakker, T.W. Primary nucleation induced by ultrasonic cavitation. *J. Cryst. Growth* **2006**, *294*, 9–15. [[CrossRef](#)]
28. Mullin, J.W. *Crystallization*, 4th ed.; Butterworth-Heinemann: Oxford, UK, 2011; p. 594.
29. Söhnel, O.; Mullin, J.W. Interpretation of crystallization induction periods. *J. Colloid Interface Sci.* **1988**, *123*, 43–50. [[CrossRef](#)]
30. Miyasaka, E.; Ebihara, S.; Hirasawa, I. Investigation of primary nucleation phenomena of acetylsalicylic acid crystals induced by ultrasonic irradiation—ultrasonic energy needed to activate primary nucleation. *J. Cryst. Growth* **2006**, *295*, 97–101. [[CrossRef](#)]
31. Monnier, H.; Wilhelm, A.M.; Delmas, H. Influence of ultrasound on mixing on the molecular scale for water and viscous liquids. *Ultrason. Sonochem.* **1999**, *6*, 67–74. [[CrossRef](#)]
32. Lee, J. Importance of sonication and solution conditions on the acoustic cavitation activity. In *Handbook of Ultrasonics and Sonochemistry*; Ashokkumar, M., Ed.; Springer: Singapore, 2016; pp. 137–175.
33. Alexander, A.J.; Camp, P.J. Single pulse, single crystal laser-induced nucleation of potassium chloride. *Cryst. Growth Des.* **2009**, *9*, 958–963. [[CrossRef](#)]
34. Mersmann, A. Calculation of interfacial tensions. *J. Cryst. Growth* **1990**, *102*, 841–847. [[CrossRef](#)]
35. Söhnel, O. Electrolyte crystal-aqueous solution interfacial tensions from crystallization data. *J. Cryst. Growth* **1982**, *57*, 101–108. [[CrossRef](#)]
36. Mullin, J.W.; Zacek, S. The precipitation of potassium aluminium sulphate from aqueous solution. *J. Cryst. Growth* **1981**, *53*, 515–518. [[CrossRef](#)]
37. Mullin, J.; Raven, K. Nucleation in agitated solutions. *Nature* **1961**, *190*, 251. [[CrossRef](#)]
38. Lee, J.; Yasui, K.; Tuziuti, T.; Kozuka, T.; Towata, A.; Iida, Y. Spatial distribution enhancement of sonoluminescence activity by altering sonication and solution conditions. *J. Phys. Chem. B* **2008**, *112*, 15333–15341. [[CrossRef](#)] [[PubMed](#)]

39. Mitome, H.; Kozuka, T.; Tuziuti, T. Measurement of the establishment process of acoustic streaming using laser Doppler velocimetry. *Ultrasonics* **1996**, *34*, 527–530. [[CrossRef](#)]
40. Lee, J.; Ashokkumar, M.; Yasui, K.; Tuziuti, T.; Kozuka, T.; Towata, A.; Iida, Y. Development and optimization of acoustic bubble structures at high frequencies. *Ultrason. Sonochem.* **2011**, *18*, 92–98. [[CrossRef](#)] [[PubMed](#)]
41. Sawamura, S.; Egoshi, N.; Setoguchi, Y.; Matsuo, H. Solubility of sodium chloride in water under high pressure. *Fluid Phase Equilib.* **2007**, *254*, 158–162. [[CrossRef](#)]
42. Hatanaka, S.; Yasui, K.; Tuziuti, T.; Kozuka, T.; Mitome, H. Quenching mechanism of multibubble sonoluminescence at excessive sound pressure. *Jpn. J. Appl. Phys.* **2001**, *40*, 3856–3860. [[CrossRef](#)]
43. Brotchie, A.; Grieser, F.; Ashokkumar, M. Effect of power and frequency on bubble-size distributions in acoustic cavitation. *Phys. Rev. Lett.* **2009**, *102*, 084302. [[CrossRef](#)] [[PubMed](#)]
44. Yasui, K. Influence of ultrasonic frequency on multibubble sonoluminescence. *J. Acoust. Soc. Am.* **2002**, *112*, 1405–1413. [[CrossRef](#)] [[PubMed](#)]



© 2018 by the authors. Licensee MDPI, Basel, Switzerland. This article is an open access article distributed under the terms and conditions of the Creative Commons Attribution (CC BY) license (<http://creativecommons.org/licenses/by/4.0/>).